Comprehensive Physico-Chemical and Functional Similarity Assessment of Intravenous and Subcutaneous RGB-19 Drug Products as Proposed Biosimilars to Tocilizumab Reference Product

Supplementary Material

BioDrugs

Katalin Solti, Sarolta Timári, Tamás Faludi, Attila Iliás, Rózsa Hegedüs, Zoltán Pataj, Viktor Háda

Biotechnology Process Development & Analytics, Biotechnology Business Unit, Gedeon Richter Plc., Gyömrői út 19-21., 1103 Budapest, Hungary

Corresponding author: Viktor Háda, v.hada@gedeonrichter.com

Table 1 Applied analytical and functional assay panel for the comparative assessment of RGB-19 proposed biosimilar to the reference product RoActemra®

Quality attribute	Applied analytical and functional assay methods
Primary structure	
Molecular mass	Intact molecular mass analysis by LC-MS
Fc/2 fragment, light chain (LC) and Fd' fragment	Subunit molecular mass analysis by LC-MS
Amino acid sequence and modifications/variants	Reduced peptide mapping analysis by LC-MS (with Lys-C enzyme)
	Reduced peptide mapping analysis by LC-MS (with Chymotrpysin enzyme)
Disulfide bridges and Cysteine variants	Non-reduced peptide mapping analysis by LC-MS (with Lys-C and Trypsin enzyme)
Free thiol	Ellman's assay
Oxidation in non-CDR (HC_Met 254)	Hotspot peptide mapping analysis by RP-UHPLC-UV (with Lys-C enzyme)
Non-glycated and monoglycated form	Intact glycation analysis by LC-MS
Glycosylation and sialylation	
Galactosylated, fucosylated, afucosylated, high mannose and sialylated forms	Hydrophilic interaction chromatography with fluorescence detection (HILIC-HPLC-FL)
Bisecting GlcNAc, Gal-α-1,3-Gal	HILIC-UHPLC-FL/ESI-MS/MS with exoglycosidase digestions
Sialylation (NANA, NGNA)	Reversed phase chromatography (RP-HPLC-FL)
Glycosylation site analysis	Non-reduced peptide mapping analysis by LC/MS (after deglycosylation)
Non-glycosylated HC (NgHC)	Reducing capillary gel electrophoresis (R-CE-SDS)
Higher order structure	
Thermodynamic stability, tertiary structure	Differential scanning calorimetry (micro-DSC)
Secondary structure	Fourier transform infrared spectroscopy (FT-IR)
Secondary structure	Circular dichroism (CD far UV)
Tertiary structure	Circular dichroism (CD near UV)
Higher order structure	Hydrogen/deuterium exchange mass spectrometry (HDX-MS)
Higher order structure	Nuclear magnetic resonance (2D NMR)
Size related variants	
High molecular weight species (HMWs)	Size exclusion chromatography (SEC-HPLC)
	Size exclusion chromatography with multi angle laser light scattering (SEC-MALLS)
	Analytical ultracentrifugation (AUC)
Low molecular weight species (LMWs)	Non-reducing capillary gel electrophoresis (NR-CE-SDS)
Charge related variants	
Acidic and basic variants	Ion exchange chromatography (IEX-HPLC)
	Ion exchange chromatography after digestion with carboxypeptidase B (IEX-HPLC after CPB digestion)
Isoelectric point	Capillary isoelectric focusing (cIEF)
Hydrophobic variants	Hydrophobic interaction chromatography (HIC-HPLC)
Biological activity	
sIL-6R binding	Enzyme-linked immunoassay (ELISA)
sIL-6R binding	Biolayer interferometry (BLI)
Dissociation of IL-6/sIL-6R complex	Enzyme-linked immunoassay (ELISA)

Quality attribute	Applied analytical and functional assay methods
Inhibition of sIL-6R mediated trans signalling	Reporter gene assay
Cell surface mIL-6R binding	Flow cytometry
IL-6/mIL-6 downstream signal neutralization (inhibition of pSTAT3)	Enzyme-linked immunoassay (ELISA)
Anti-proliferation assay	Cell-based assay in TF-1 cell
FcRn binding	Biolayer interferometry (BLI)
C1q binding	Biolayer interferometry (BLI)*
FcγRI (CD64) binding	Biolayer interferometry (BLI)*
FcγRIIa (CD32a) binding	Biolayer interferometry (BLI)*
FcγRIIIa (CD16a) binding	Biolayer interferometry (BLI)*
Antibody-dependent cell-mediated cytotoxicity (ADCC)	ADCC reporter gene assay
Complement-dependent cytotoxicity (CDC)	Cell-based assay
Composition and strengths	
Protein content	UV spectrophotometry
Subvisible particles	
Number of subvisible particles (SVP)	Resonant mass measurement (RMM)
	Light obscuration (LO)

Gray background indicates the methods whose descriptions, measurement results and figures are given here, in the Supplementary material

*Method description is given in the main text as a merged description together with other BLI methods

Analytical Methods for Protein Characterization

Differential Scanning Calorimetry (DSC)

DSC was used to determine the melting point (unfolding-folding transition temperature) and the unfolding enthalpy change, which provides insights into the tertiary structure. Thermograms were recorded using an automated MicroCal AutoPEAQ-DSC® (Malvern Instruments, Malvern, UK). Auto PEAK software was used to process and analyze the melting temperature. For thermogram evaluation, baseline correction was performed using the spline fitting method.

FT-IR Spectroscopy

All FT-IR spectra were collected using an attenuated total reflection Fourier-transform infrared spectrophotometer (PerkinElmer Instruments, Spectrum 3 MIR), running Spectrum ES 10 software. All spectra were recorded at room temperature with the resolution of 4 cm^{-1} in the wavenumber range 4000-650 cm^{-1}. After baseline correction, smooth processing and normalization, the second derivative spectra with 13 points were calculated.

Circular Dichroism Spectroscopy, CD Far UV and Near UV

Measurements were performed on a JASCO (Tokyo, Japan) J-1500 Automated Circular Dichroism spectrometer. Secondary and tertiary structures were evaluated at 1.5 mg/mL in the far UV region (195-260 nm) and 20 mg/mL in the near UV region (250-320 nm), and cell temperature was 20 °C. The Spectra Analysis evaluation module of the Spectra Manager software was used for baseline correction. The Peak Find function was used to manually

identify the characteristic maxima and minima in the near UV region, indicative of tertiary structure. The secondary structure was predicted using the CD Multivariate SSE program built into Spectra Manager.

High Molecular Weight Species (HMWs) by Size Exclusion Chromatography with Multi Angle Laser Light Scattering (SEC-MALLS)

Samples were separated using a Tosoh Bioscience TSKgel G3000SWXl analytical column (7.8 × 300 mm, 5 µm, Tosoh) together with a Tosoh Bioscience TSKgeI SWXL Guard precolumn (6.0 × 40 mm, 7 µm, Tosoh) on an Agilent 1260 Infinity II HPLC instrument equipped with a miniDAWN light scattering detector (Wyatt) and a refractive index detector (Shodex 501, Shodex). Chromatographic parameters: ambient temperature, flow rate: 0.5 mL/minute, isocratic elution (100mM sodium phosphate, 250mM sodium sulfate, pH 6.8), UV detection: 280 nm, MALLS detection: 660 nm, RI detection: 800 nm. Data were collected and processed using ASTRA software (Wyatt) to determine the absolute molecular weight values.

Sedimentation Velocity by Analytical Ultracentrifugation (SV-AUC)

The analysis was performed using a ProteomeLab XL-I instrument (Beckman Coulter), equipped with an 8-hole AN 50 Ti rotor. Runs were carried out using cells with quartz windows and 12-mm path length charcoal-filled epon centerpieces (Beckman Coulter). 120 scans were collected for each cell. Data was analysed using a continuous distribution c(s) model in Sedfit 16.1.

Identity Test by Capillary Isoelectric Focusing (cIEF)

The samples were separated in an ampholyte-containing matrix (Pharmalyte 3-10, Sigma) using a Maurice S. CE instrument (ProteinSimple) with dedicated cIEF cartridge. UV detection was performed using Compass for iCE software (ProteinSimple v 2.1.0). The basis for the assessment of identity was the isoelectric points (pI) of the tested samples, which were determined based on the position of the pI markers (pI 8.40 and pI 10.17 from ProteinSimple). The samples were considered identical, if the difference between the isoelectric points was not more than 0.03 pI.

Hydrophobic Variants by Hydrophobic Interaction Chromatography (HIC-HPLC)

Separation was performed using a Thermo MabPac HIC (4.6 × 250 mm, 5 µm) column (Thermo) on a Shimadzu Nexera HPLC system under non-denaturing conditions. Chromatographic parameters: column temperature: 37°C, flow rate: 1.0 mL/minute, gradient elution (Eluent A: 1.8 M $(NH_4)_2SO_4$ + 0.2 M NaH_2PO_4 pH=7.0, Eluent B: 0.2 M NaH_2PO_4 pH= 7.0), UV detection: 214 nm. Data collection was performed using LabSolutions CS 6.88 SP1 (Shimadzu) software, and the area percentage of main peak, prepeaks and postpeaks were evaluated.

<u>Functional Assays</u>

Dissociation of IL-6/sIL-6R Complex by ELISA

sIL-6R (Peprotech) was preincubated with IL-6 (Peprotech) and then varying concentrations of test samples were added. The detection of the resulting tocilizumab/sIL-6R complex was performed on an ELISA plate coated with a non-neutralizing anti-human sIL-6R antibody (Diaclone). The amount of the tocilizumab/sIL-6R complex was

determined using AP-conjugated anti-human IgG (Merck-Millipore) and the chromogenic p-nitrophenyl phosphate (pNPP) substrate (Merck) by using Synergy Neo 2 microplate reader (BioTek). The evaluation was based on the comparison of the dose-response curves obtained from the dilution series and results were evaluated using the PLA software (Stegmann Systems). Relative biological activity was calculated from the EC50 values of the curves.

Inhibition of Trans-signalling Activity of IL-6/sIL-6R Complex by Cell-based Luciferase Reporter Gene Assay

A genetically modified cell line (HEK293/Stat3-RE-Luc2P + mIL6R KO, Promega) expressing gp130 on the cell surface and being only capable of trans-signalling was used. sIL-6R (Peprotech) was preincubated with IL-6 (Peprotech) and then test samples of varying concentrations were added. The resulting complex was incubated with the cells seeded on microplates, and the emerging bioluminescent signal was detected by the addition of luciferase substrate and quantified using a Synergy Neo 2 microplate reader (BioTek). The results were evaluated using the PLA software (Stegmann Systems), which calculates the relative biological activity of the sample from the EC50 value of the curves.

Inhibition of STAT3 Phosphorylation by Cell-based ELISA

Hep G2 (ATCC) cells, expressing mIL-6R on the surface, were treated with serial dilutions of the test sample. Then, the cells were incubated with a constant concentration of rhIL-6 (Peprotech). After cell lysis, phosphorylated STAT3 (pSTAT3) was measured using a commercially available sandwich ELISA kit (Cell Signaling Technology). The detection was performed using a Synergy Neo 2 microplate reader (BioTek). The results were evaluated using the PLA software (Stegmann Systems), which calculated the relative biological activity of the sample from the EC50 value of the curves.

Antibody-dependent Cellular Cytotoxicity (ADCC) by a Reporter Gene Assay

An IL-6 receptor expressing DS-1 cell line (ATCC) was used as target cell. FcγRIIIa (V158) expressing effector cells (Promega) attach to the Fc region of the target cell-bound antibody of interest. The binding activates an intracellular signalling cascade, resulting in the induction of NFAT-mediated luciferase expression in the effector cells. After the addition of luciferase substrate, the bioluminescent light produced by the cells was measured using a Synergy Neo 2 microplate reader (BioTek). Since no measurable ADCC activity is expected from test samples, an appropriate positive control, anti-HLA1 IgG1 antibody (Absolute antibody) was used. Evaluation was performed using Gen5 Secure software (BioTek), which plotted the measured logarithmic luminescence values as a function of concentration on a logarithmic scale. A 4PL curve was fitted to the anti-HLA1 treatment data points, while the curve fitted to the data points of the test samples was nearly parallel to the x-axis due to the lack of effect.

Complement-dependent Cytotoxicity (CDC) Assay

DS-1 cells (ATCC), which express high levels of IL-6 receptor on the surface, were treated with varying concentrations of test samples, followed by the addition of human serum complement (Quidel). The resulting antibody-antigen complex activated the complement system, leading to the destruction of the target cells.

Surviving cells were quantified through the addition of PrestoBlue reagent (Life Technologies) and subsequent detection using the Synergy Neo 2 microplate reader (BioTek). The assay included a positive control antibody (anti-HLA1, Absolute antibody) that was shown to induce CDC. Evaluation was based on Gen5 Secure software (BioTek) which fitted a 5PL curve to the anti-HLA1 data points, while the curve fitted to the data points of the test samples was nearly parallel to the x-axis due to the lack of effect.

Analytical Methods for Protein Content and Particles

Protein Content by UV Spectrophotometry

Sample preparation was carried out using gravimetric dilution, and the dilution factor was determined based on the resulting mass data. Absorbance was determined between 240 and 350 nm using UV-2600 spectrophotometer with LabSolutions CS 6.88 SP1 software (Shimadzu). The applied extinction coefficient was determined by amino acid analysis. Protein content was calculated as the average of three parallel sample preparations.

Subvisible Particles by Resonant Mass Measurement (RMM)

Analyses were performed using an Archimedes particle metrology system (Malvern Instruments Ltd, Malvern, Worcestershire, UK) equipped with a Hi-Q Micro Sensor and controlled by Archimedes 1.20 software. Between sample runs, the system was rinsed, and a cleaning test was run. The limit of detection (LOD) was determined in automatic LOD mode.

Subvisible Particles by Light Obscuration (LO)

Analyses were performed using PAMAS SVSS (PAMAS GmbH, Rutesheim, Germany) particle counting system equipped with an HCB-LD-25/25 sensor. Aliquots of pooled samples were analysed, depending on the packaging unit. The results were reported as mean particle concentration.

Figures and Tables

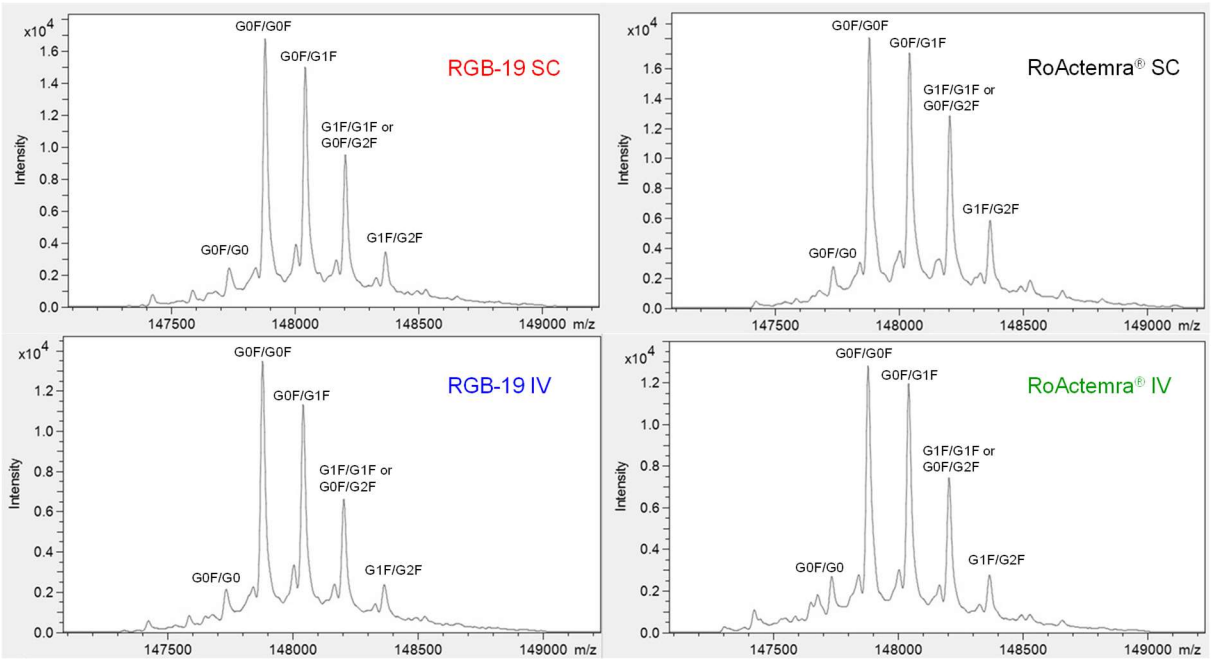

Fig. 1 Representative deconvoluted intact mass spectra obtained from the on-line RP-HPLC/ESI-MS analysis of the intact tocilizumab in intravenous (IV) and subcutaneous (SC) drug product batches of RGB-19 and RoActemra®

Table 2 Summary of the data obtained from the on-line RP-HPLC/ESI-MS intact molecular mass analysis of the intact tocilizumab in IV and SC drug product batches of RGB-19 and RoActemra®. C-terminal lysine is absent, and the N-terminal glutamine amino acids of both heavy chains appear in pyro-glutamate form

Form / sample	Theoretical average molecular mass [Da]	Measured average molecular mass [Da]			
		RGB-19 IV	RoActemra® IV	RGB-19 SC	RoActemra® SC
G0F/G0	147729.8	147732.9	147733.5	147733.1	147733.0
G0F/G0F	147876.0	147878.2	147878.7	147878.1	147878.5
G0F/G1F	148038.1	148040.3	148040.6	148040.3	148040.8
G1F/G1F or G0F/G2F	148200.2	148202.5	148202.9	148202.3	148202.9
G1F/G2F	148362.4	148364.4	148364.7	148364.8	148365.0

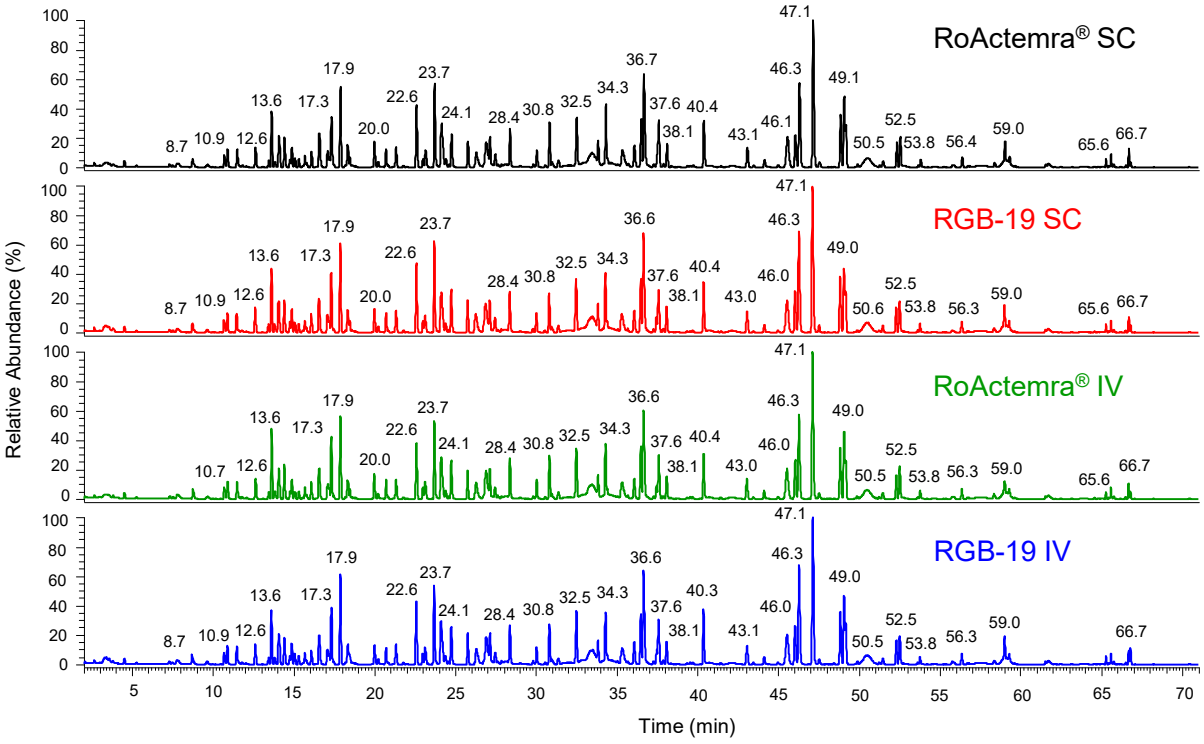

Fig. 2 Base peak chromatograms of IV and SC drug product batches of RGB-19 and RoActemra® obtained during the on-line RP-HPLC/ESI-MS/MS analysis of the chymotrypsin digested tocilizumab under reducing conditions

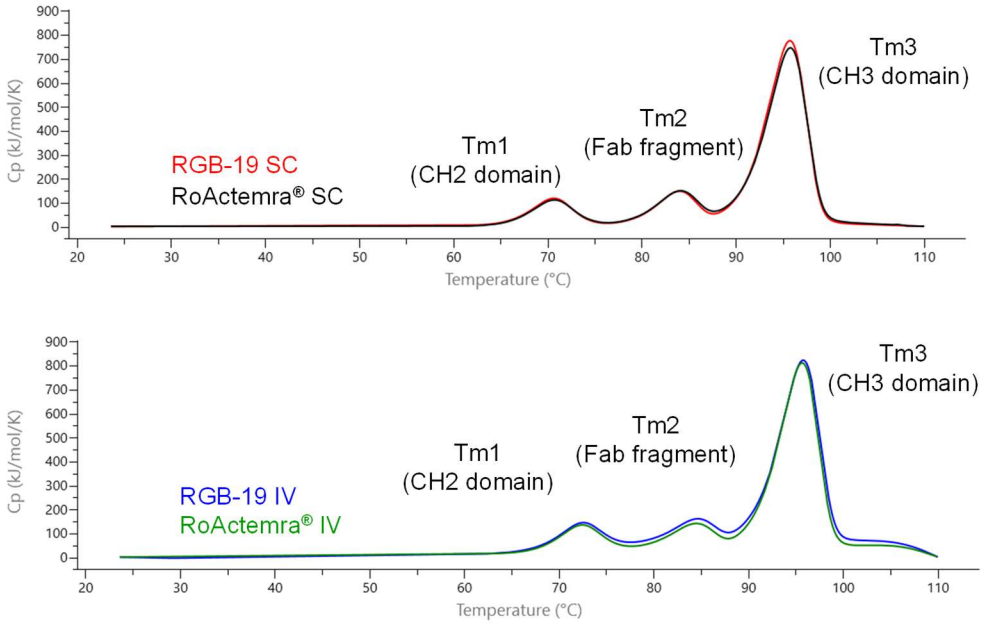

Fig. 3 µDSC thermograms of IV and SC drug product batches of RGB-19 and RoActemra®

Table 3 Summary of the quantitative analytical data of µDSC analyses of the IV and SC presentations of the RGB-19 proposed biosimilar and reference product RoActemra® batches

Attribute	RGB-19 IV Min-Max range (n)	RoActemra® IV Quality range (n)	RGB-19 SC Min-Max range (n)	RoActemra® SC Quality range (n)
Higher order structure				
µDSC				
Tm1 (°C)	72.39-72.46 (6)	72.15-72.56 (40)	70.52-70.70 (5)	69.82-71.32 (22)
Tm2 (°C)	84.44-84.53 (6)	84.30-84.50 (40)	83.89-83.96 (5)	83.60-84.55 (22)
Tm3 (°C)	95.54-95.66 (6)	95.17-96.09 (40)	95.59-95.65 (5)	94.98-96.23 (22)
ΔH (kJ/mol)	6720-7670 (6)	5543-7281 (40)	5880-6480 (5)	5035-7683 (22)

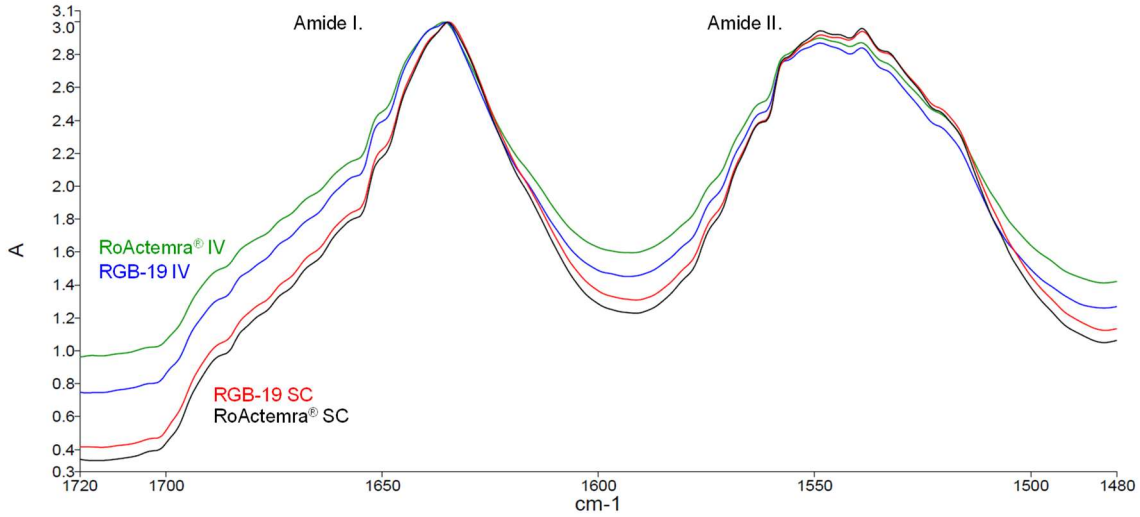

Fig. 4 FT-IR spectra of IV and SC drug product batches of RGB-19 and RoActemra®

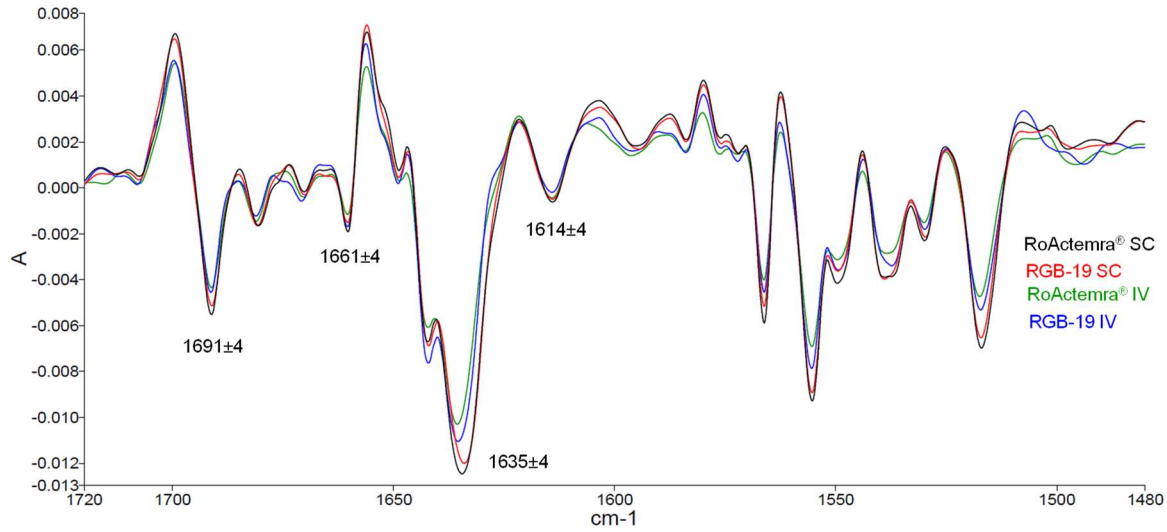

Fig. 5 FT-IR spectra (second derivative) of IV and SC drug product batches of RGB-19 and RoActemra®

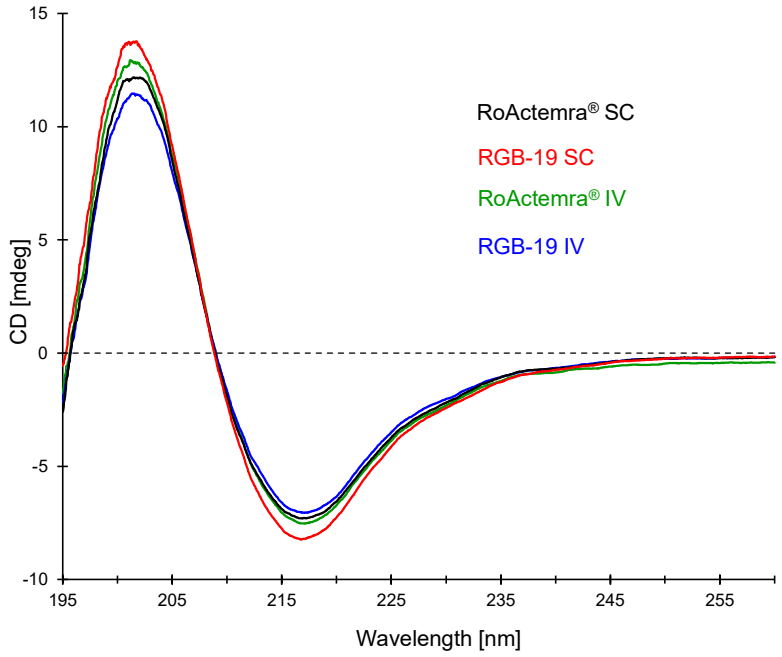

Fig. 6 CD far UV spectra of IV and SC drug product batches of RGB-19 and RoActemra®

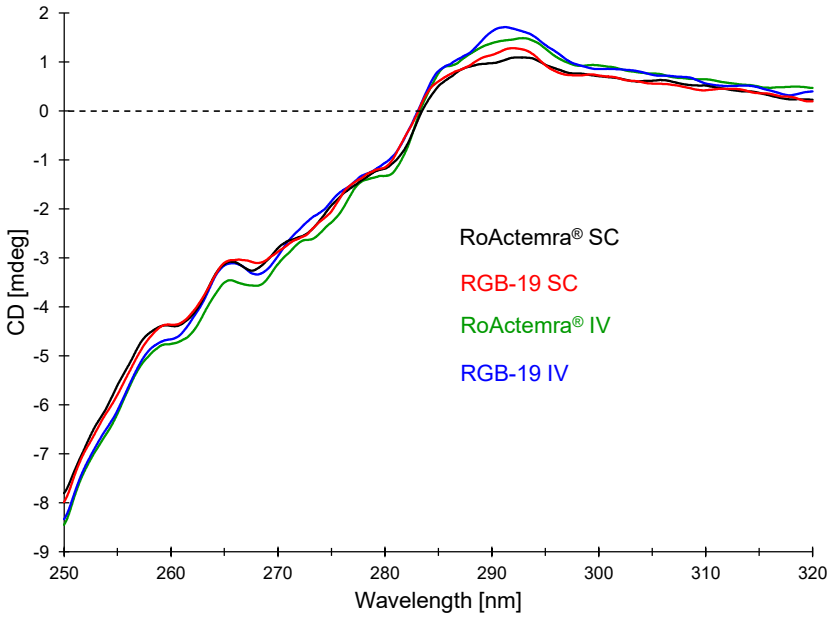

Fig. 7 CD near UV spectra of IV and SC drug product batches of RGB-19 and RoActemra®

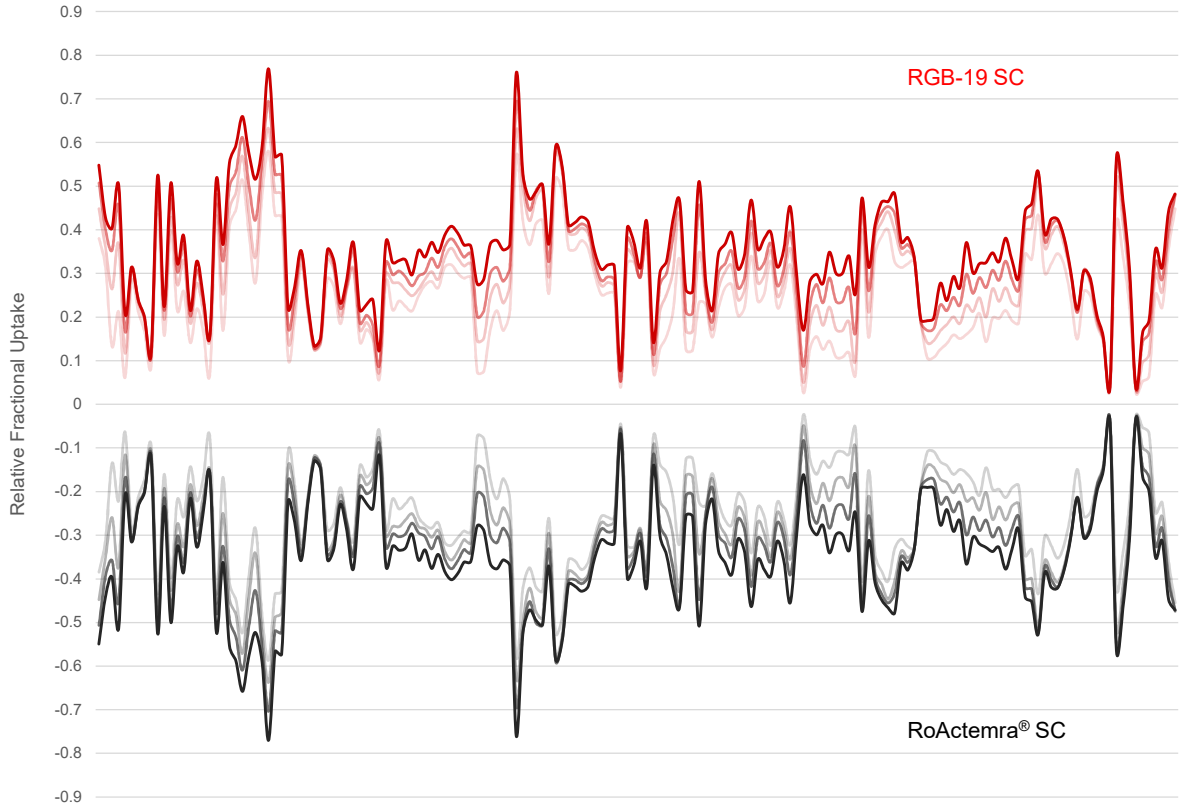

Fig. 8 Fractional deuterium uptake plot ("butterfly-plot") for the comparison of the deuterium uptakes of tocilizumab HC peptides between the examined RGB-19 SC and RoActemra® SC product batches. Shades of red: RGB-19 SC fractional deuterium uptake plots acquired for four different deuteration intervals; shades of black: RoActemra SC® fractional deuterium uptake plots acquired for four different deuteration intervals (the same as for RGB-19 SC)

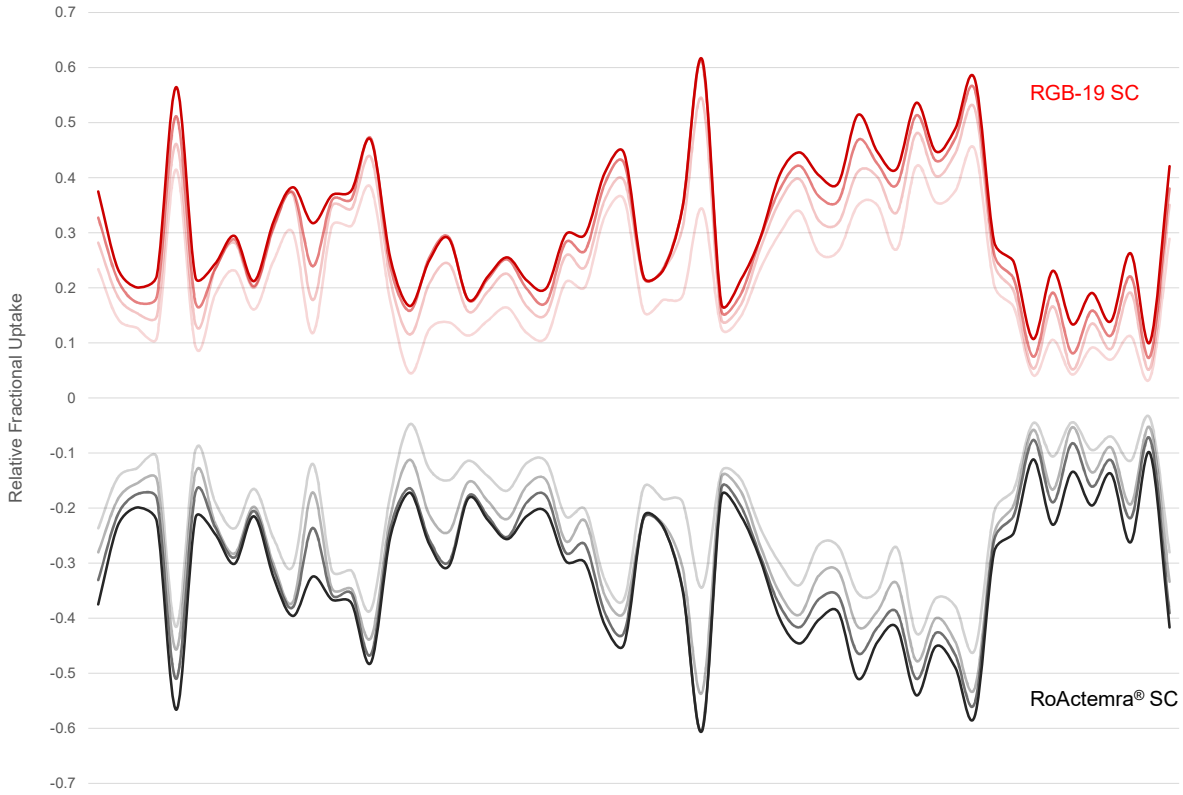

Fig. 9 Fractional deuterium uptake plot ("butterfly-plot") for the comparison of the deuterium uptakes of tocilizumab LC peptides between the examined RGB-19 SC and RoActemra® SC product batches. Shades of red: RGB-19 SC fractional deuterium uptake plots acquired for four different deuteration intervals; shades of black: RoActemra SC® fractional deuterium uptake plots acquired for four different deuteration intervals (the same as for RGB-19 SC)

Chemometric evaluation of 2D NMR data:

In order to provide a quantitative measure of spectral similarity as an objective approach in addition to visual comparison, well-resolved protein-related methyl signals were peak picked and the chemical shift data was analyzed further. Combined chemical shift differences (CCSDs) were calculated and compared pairwise. Exact chemical shifts of peak maxima of 54 well-resolved ^{1}H-^{13}C 2D correlation peaks were extracted using MestReNova's automatic peak picking algorithm. Corresponding crosspeaks between spectra were manually reviewed and curated if needed (i. e. in case of erroneous picking of noise, missing peaks, inverted peak order, etc). CCSDs of individual spectra were calculated according to the following formula[1]:

$$CCSD = \sqrt{\frac{1}{2}\left[\left(\delta_{1_H} - \delta_{1_{H,ref}}\right)^2 + \left(0.251 \cdot \delta_{13_C} - 0.251 \cdot \delta_{13_{C,ref}}\right)^2\right]}$$

Since CCSD is suitable for pairwise spectral comparison, for determination of CCSD values for all spectra, a reference peak list was generated from the spectrum of a randomly selected RoActemra® sample. Then, CCSD values of all aquired RoActemra® spectra were averaged and corresponding standard deviations were calculated. The average CCSD plus three times of standard deviation (3SD) served as measure of batch-to-batch spectral variation (with experimental error added) of chemical shifts of the corresponding peak (shown as positive error bars). These limit values were then compared with the averaged CCSD values of corresponding peak pairs of duplicate RGB-19 samples. As shown in Fig. 10, none of the observed CCSDs calculated for peak-pairs of spectra of RGB-19 SC samples exceeded the average plus three times of standard deviation. This statistical evaluation of pairwise chemical shift differences suggest that the higher order structure of each protein drug substance investigated in this study is similar to each other.

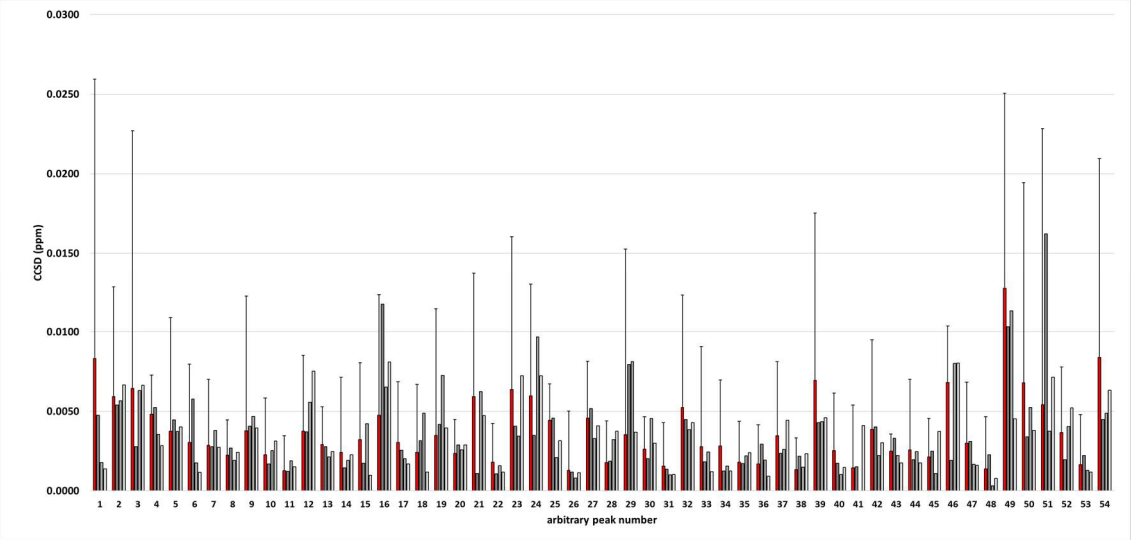

Fig. 10 CCSD values of methyl peaks as the function of arbitrary peak numbers. Averaged CCSD plus 3SD values are shown with red bars and positive error bars, average CCSD of NMR spectra of three batches of duplicated RGB-19 SC samples are shown with grey bars

[1] Brinson RG, Arbogast LW, Marino JP, Delaglio F. Best Practices in Utilization of 2D-NMR Spectral Data as the Input for Chemometric Analysis in Biopharmaceutical Applications. J. Chem. Inf. Model. 2020;60:2339-2355. https://pubs.acs.org/doi/full/10.1021/acs.jcim.0c00081.

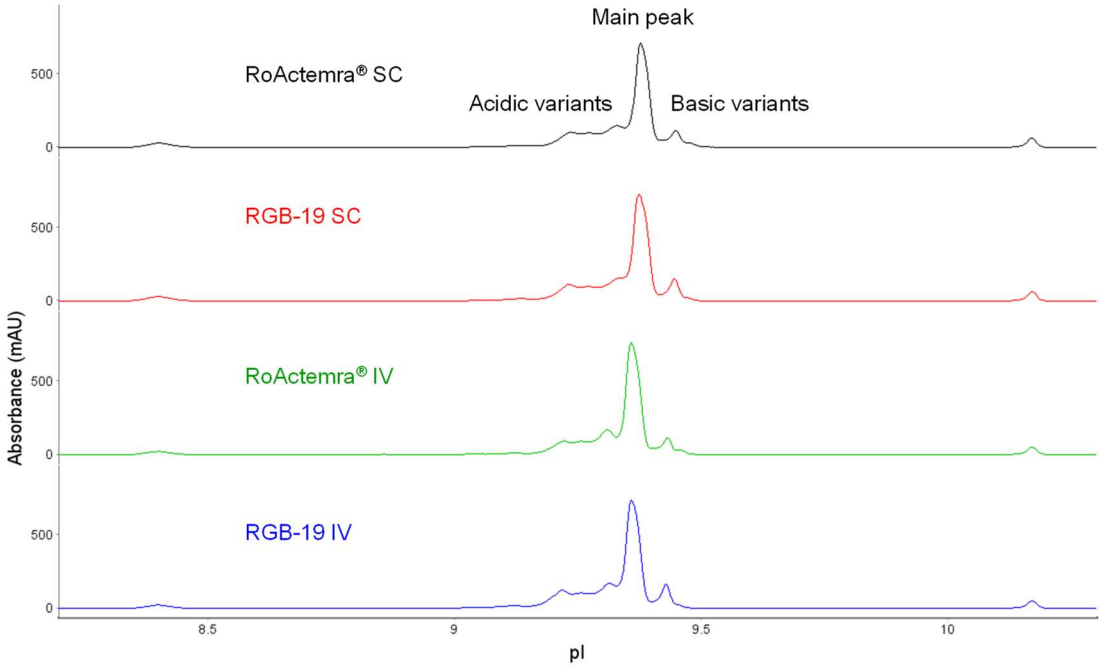

Fig. 11 cIEF electropherograms of IV and SC drug product batches of RGB-19 and RoActemra®

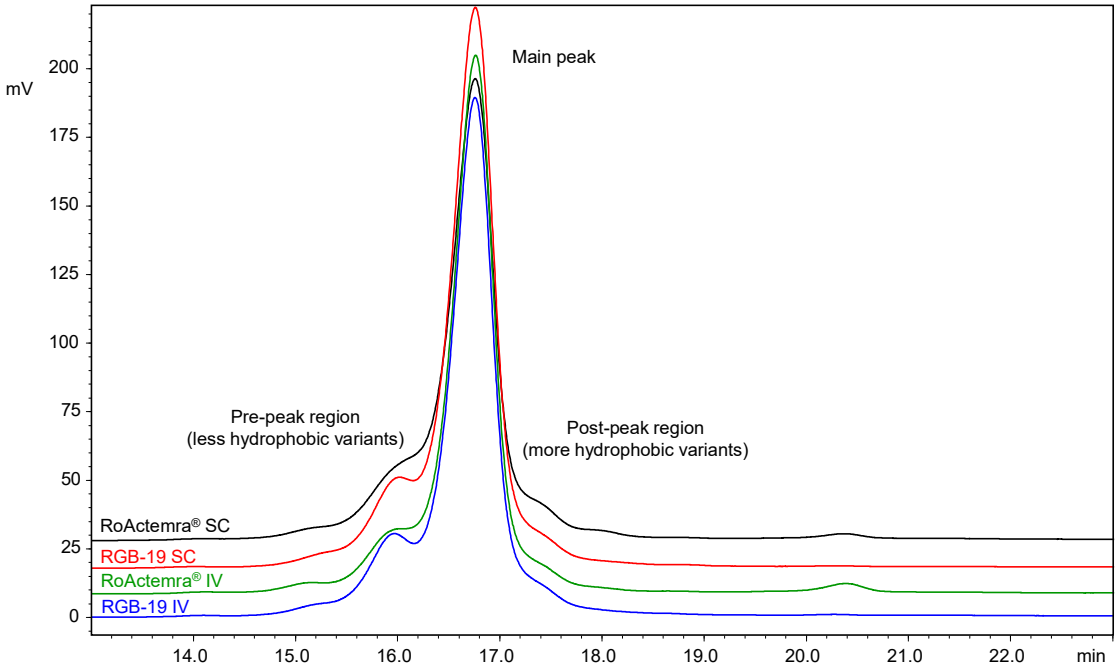

Fig. 12 HIC-HPLC chromatograms of IV and SC drug product batches of RGB-19 and RoActemra®

Table 4 Summary of the quantitative analytical data of size- and charge related, and hydrophobic variants of the IV and SC presentations of the RGB-19 proposed biosimilar and reference product RoActemra® batches

Attribute	RGB-19 IV Min-Max range (n)	RoActemra® IV Quality range (n)	RGB-19 SC Min-Max range (n)	RoActemra® SC Quality range (n)
Size related variants				
SEC-MALLS (kDa)				
HMWs	282.5-379.8 (6)	226.7-425.2 (13)	232.3-314.8 (4)	199.8-363.5 (11)
Monomer	138.4-139.0 (6)	131.6-149.6 (13)	139.2-139.9 (4)	138.5-140.3 (11)
AUC				
Monomer (area%)	94.75-96.61 (6)	90.12-99.89 (19)	95.68-96.77 (5)	91.92-98.14 (16)
Monomer (kDa)	140-145 (6)	138-152 (19)	143-148 (5)	138-148 (16)
Sedimentation coefficient (s)	5.29-5.35 (6)	5.23-5.38 (19)	5.87-5.92 (5)	5.87-5.96 (16)
Charge related variants				
pI of main peak / cIEF	9.35-9.36 (6)	9.32-9.37 (39)*	9.37-9.38 (5)	9.34-9.38 (19)*
Hydrophobic variants				
HIC (area%)				
Prepeak	13.4-15.0 (6)	7.8-16.8 (34)	12.9-13.7 (5)	10.6-16.4 (18)
Postpeak	3.8-4.8 (6)	2.4-10.8 (34)	6.0-7.3 (5)	2.9-11.6 (18)
Main peak	80.2-82.7 (6)	76.0-86.2 (34)	79.2-81.1 (5)	73.6-84.9 (18)

*QR was established based on min-max values to demonstrate similarity

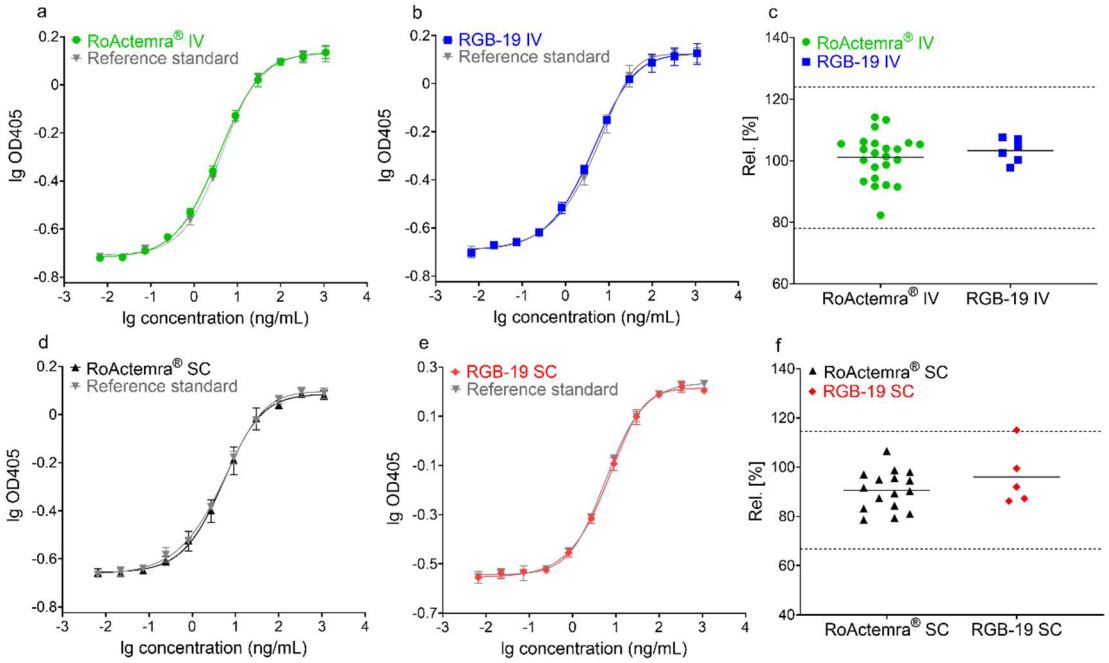

Fig. 13 Dissociation activity to IL-6/sIL-6R complex of RoActemra® and RGB-19 IV and SC batches. Representative dose-response curves of **(a)** RoActemra® IV, **(b)** RGB-19 IV; **(c)** comparison of dissociation activity to IL-6/sIL-6R complex of RoActemra® IV and RGB-19 IV batches. Representative dose-response curves of **(d)** RoActemra® SC, **(e)** RGB-19 SC; **(f)** comparison of dissociation activity to IL-6/sIL-6R complex of RoActemra® SC and RGB-19 SC batches. Dashed lines: upper and lower limits of quality ranges

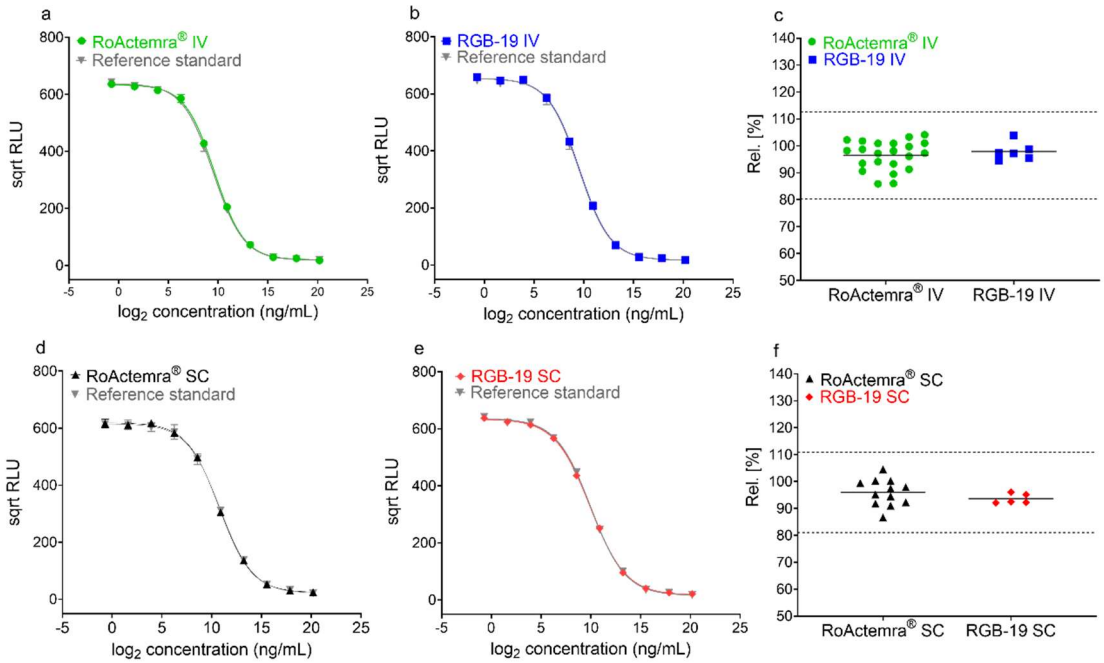

Fig. 14 Inhibition of sIL-6R mediated trans-signalling in RoActemra® and RGB-19 IV and SC batches. Representative dose-response curves of **(a)** RoActemra® IV, **(b)** RGB-19 IV; **(c)** comparison of inhibition of sIL-6R mediated trans-signalling in RoActemra® IV and RGB-19 IV batches. Representative dose-response curves of **(d)** RoActemra® SC, **(e)** RGB-19 SC; **(f)** comparison of inhibition of sIL-6R mediated trans-signalling in RoActemra® SC and RGB-19 SC batches

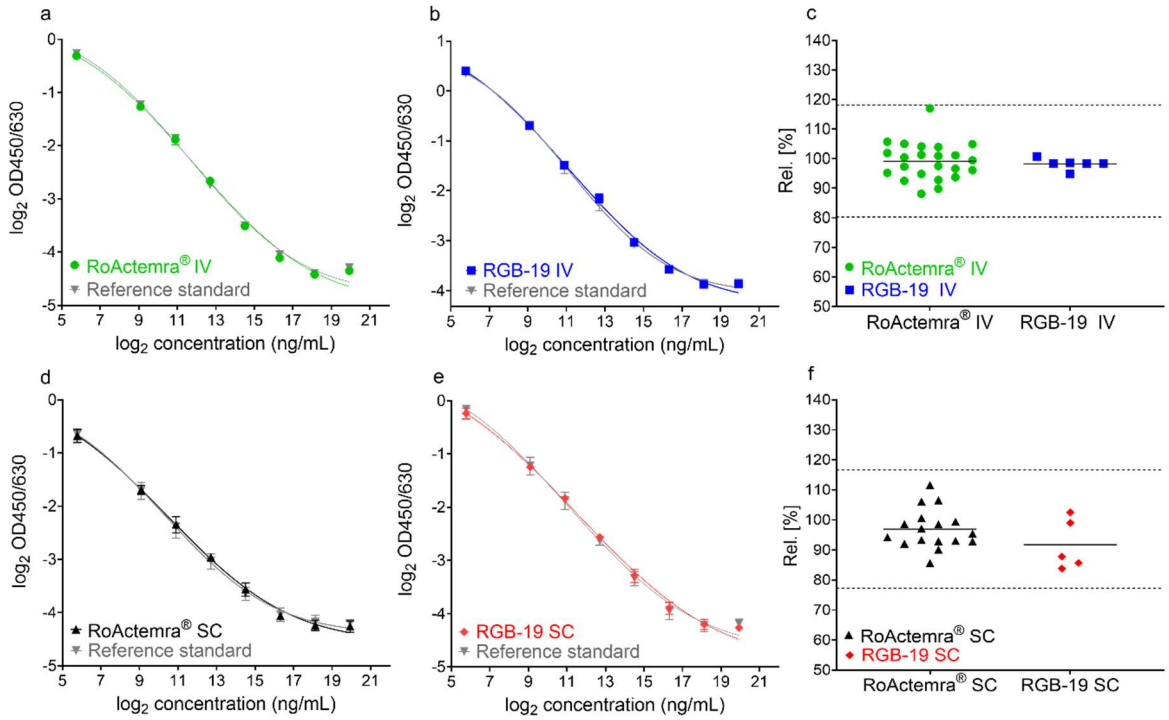

Fig. 15 The inhibition of STAT3 phosphorylation in RoActemra® and RGB-19 IV and SC batches. Representative dose-response curves of **(a)** RoActemra® IV, **(b)** RGB-19 IV; **(c)** comparison of the inhibition of STAT3 phosphorylation in RoActemra® IV and RGB-19 IV batches. Representative dose-response curves of **(d)** RoActemra® SC, **(e)** RGB-19 SC; **(f)** comparison of the inhibition of STAT3 phosphorylation in RoActemra® SC and RGB-19 SC batches. Dashed lines: upper and lower limits of quality ranges

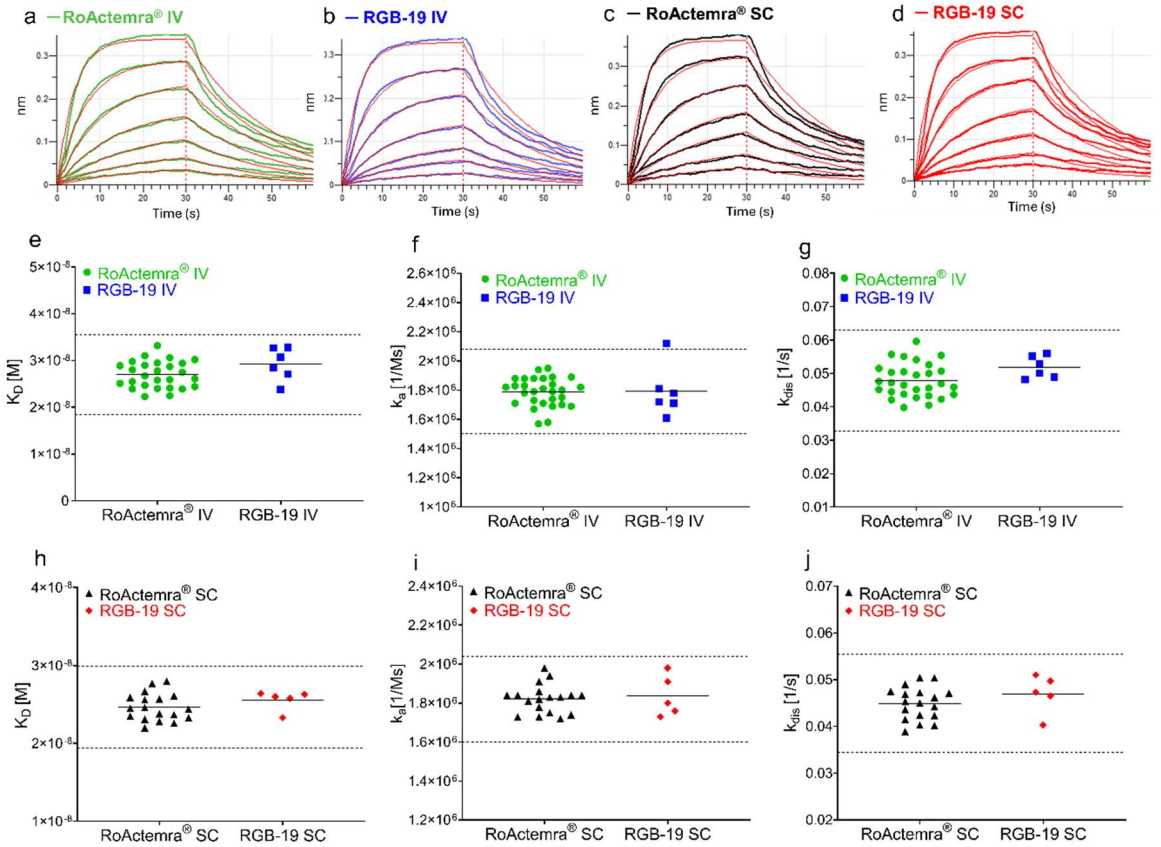

Fig. 16 C1q binding affinity of RoActemra® and RGB-19 IV and SC batches. Representative sensorgrams of **(a)** RoActemra® IV, **(b)** RGB-19 IV; **(c)** RoActemra® SC, **(d)** RGB-19 SC. Comparison of the kinetic parameters of the tocilizumab-C1q interaction: **(e)** the equilibrium dissociation constant (K_D) of RoActemra® IV and RGB-19 IV batches, **(f)** association rate constant (k_a) of RoActemra® IV and RGB-19 IV batches, **(g)** dissociation rate constant (k_{dis}) of RoActemra® IV and RGB-19 IV batches; **(h)** K_D of RoActemra® SC and RGB-19 SC batches, **(i)** k_a of RoActemra® SC and RGB-19 SC batches **(j)** k_{dis} of RoActemra® SC and RGB-19 SC batches. Dashed lines: upper and lower limits of quality ranges

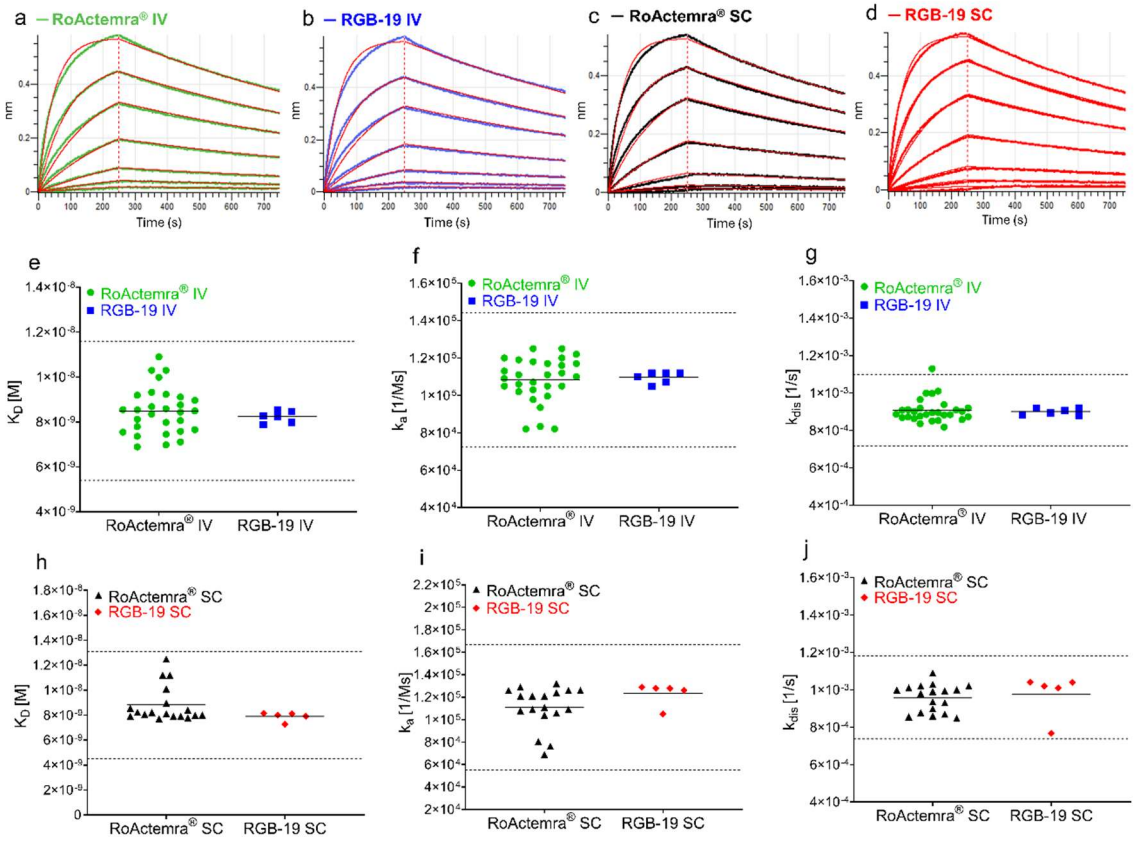

Fig. 17 FcγRI/CD64 receptor binding of RoActemra® and RGB-19 IV and SC batches. Representative sensorgrams of **(a)** RoActemra® IV, **(b)** RGB-19 IV; **(c)** RoActemra® SC, **(d)** RGB-19 SC. Comparison of the kinetic parameters of the tocilizumab-CD64 interaction: **(e)** K_D of RoActemra® IV and RGB-19 IV batches, **(f)** k_a of RoActemra® IV and RGB-19 IV batches, **(g)** k_{dis} of RoActemra® IV and RGB-19 IV batches; **(h)** K_D of RoActemra® SC and RGB-19 SC batches, **(i)** k_a of RoActemra® SC and RGB-19 SC batches **(j)** k_{dis} of RoActemra® SC and RGB-19 SC batches. Dashed lines: upper and lower limits of quality ranges

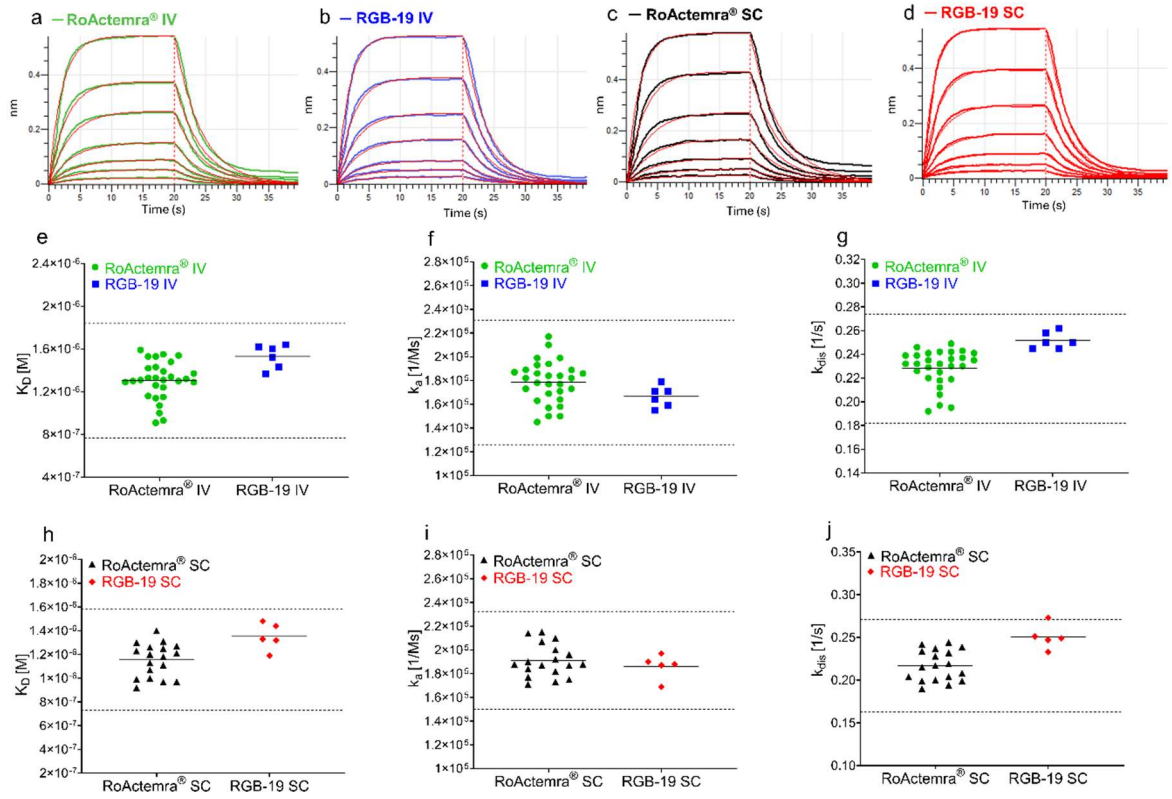

Fig. 18 FcγRIIa_R131/CD32a_R131 a receptor binding of RoActemra® and RGB-19 IV and SC batches. Representative sensorgrams of **(a)** RoActemra® IV, **(b)** RGB-19 IV; **(c)** RoActemra® SC, **(d)** RGB-19 SC. Comparison of the kinetic parameters of the tocilizumab-CD32a interaction: **(e)** K_D of RoActemra® IV and RGB-19 IV batches, **(f)** k_a of RoActemra® IV and RGB-19 IV batches, **(g)** k_{dis} of RoActemra® IV and RGB-19 IV batches; **(h)** K_D of RoActemra® SC and RGB-19 SC batches, **(i)** k_a of RoActemra® SC and RGB-19 SC batches **(j)** k_{dis} of RoActemra® SC and RGB-19 SC batches. Dashed lines: upper and lower limits of quality ranges

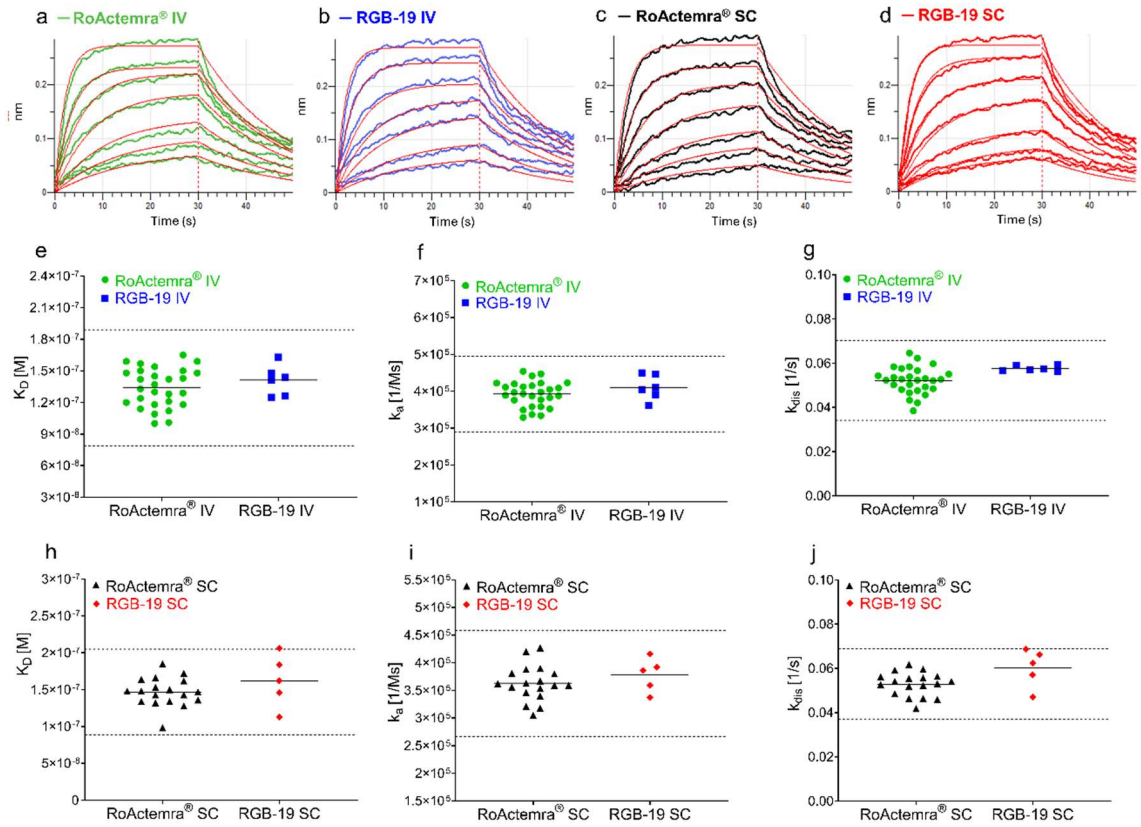

Fig. 19 FcγRIIIa_V158/CD16a_V158 a receptor binding of RoActemra® and RGB-19 IV and SC batches. Representative sensorgrams of **(a)** RoActemra® IV, **(b)** RGB-19 IV; **(c)** RoActemra® SC, **(d)** RGB-19 SC. Comparison of the kinetic parameters of the tocilizumab-CD16a interaction: **(e)** K_D of RoActemra® IV and RGB-19 IV batches, **(f)** k_a of RoActemra® IV and RGB-19 IV batches, **(g)** k_{dis} of RoActemra® IV and RGB-19 IV batches; **(h)** K_D of RoActemra® SC and RGB-19 SC batches, **(i)** k_a of RoActemra® SC and RGB-19 SC batches **(j)** k_{dis} of RoActemra® SC and RGB-19 SC batches. Dashed lines: upper and lower limits of quality ranges

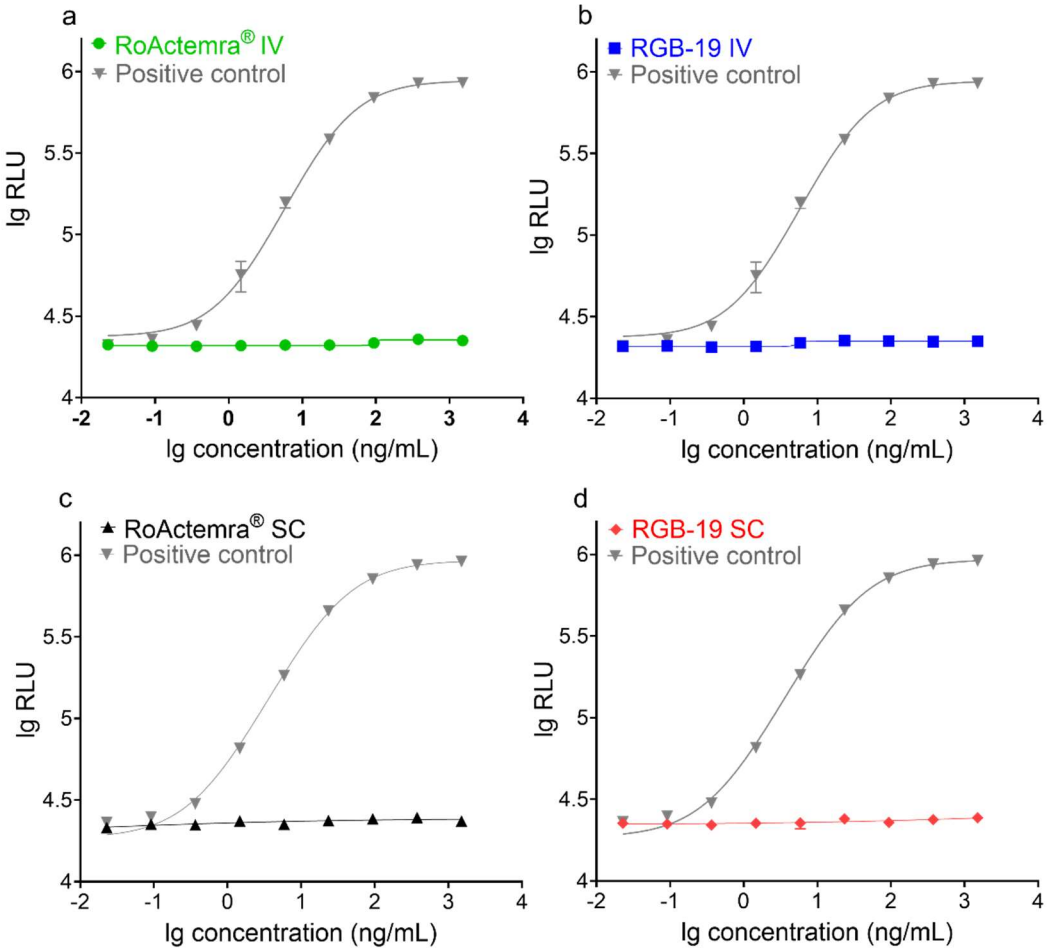

Fig. 20 Representative ADCC dose response curves of **(a)** RoActemra® IV, **(b)** RGB-19 IV, **(c)** RoActemra® SC, **(d)** RGB-19 SC batches

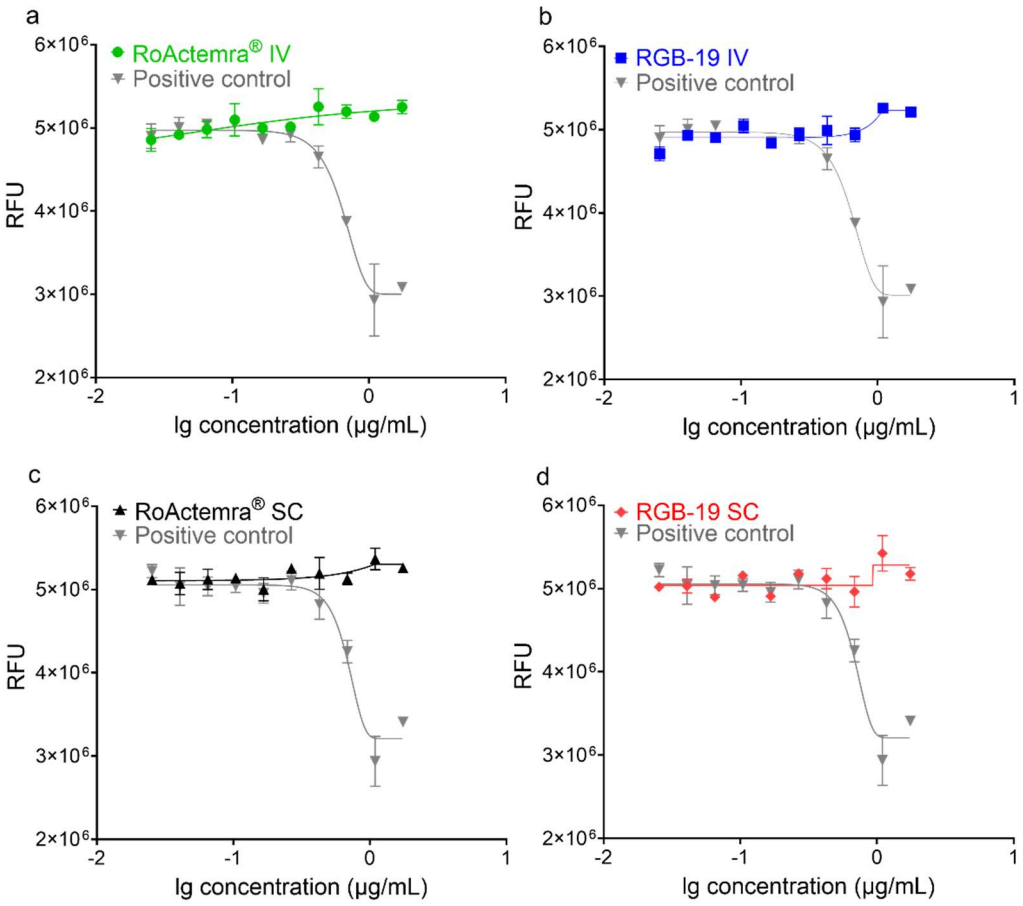

Fig. 21 Representative CDC dose response curves of **(a)** RoActemra® IV, **(b)** RGB-19 IV, **(c)** RoActemra® SC, **(d)** RGB-19 SC batches

Table 5 Summary of the quantitative functional assay data of the IV and SC presentations of the RGB-19 proposed biosimilar and reference product RoActemra® batches (K_D: the equilibrium dissociation constant; k_a: association rate constant; k_{dis}: dissociation rate constant)

Attribute	RGB-19 IV Min-Max range (n)	RoActemra® IV Quality range (n)	RGB-19 SC Min-Max range (n)	RoActemra® SC Quality range (n)
Dissociation activity to IL-6/sIL-6R complex by ELISA				
Biological activity (rel. %)	97.7-107.6 (6)	78.1-124.0 (23)	86.3-115.1 (5)	66.8-114.5 (16)
Inhibition of sIL-6R mediated trans signalling				
Biological activity (rel. %)	94.6-103.8 (6)	80.4-112.6 (22)	92.2-111.2 (5)	81.0-110.9 (12)
Inhibition of tocilizumab STAT3 phosphorylation by ELISA				
Biological activity (rel. %)	94.9-100.7 (6)	80.2-118.1 (23)	83.8-102.5 (5)	77.3-116.6 (17)
C1q binding affinity by BLI				
K_D (M)	2.38E-08-3.28E-08 (6)	1.84E-08-3.52E-08 (29)	2.33E-08-2.64E-08 (5)	1.94E-08-2.99E-08 (18)
k_a (1/Ms)	1.61E+06-2.12E+06 (6)	1.50E+06-2.08E+06 (29)	1.73E+06-1.98E+06 (5)	1.60E+06-2.04E+06 (18)
k_{dis} (1/s)	4.82E-02-5.60E-02 (6)	3.27E-02-6.30E-02 (29)	4.03E-02-5.10E-02 (5)	3.45E-02-5.54E-02 (18)
FcγRI/CD64 receptor binding affinity by BLI				
K_D (M)	7.88E-09-8.55E-09 (6)	5.40E-09-1.16E-08 (29)	7.27E-09-8.16E-09 (5)	4.53E-09-1.31E-08 (18)
k_a (1/Ms)	1.05E+05-1.12E+05 (6)	7.23E+04-1.44E+05 (29)	1.05E+05-1.29E+05 (5)	5.51E+04-1.67E+05 (18)
k_{dis} (1/s)	8.80E-04-9.21E-04 (6)	7.17E-04-1.10E-03 (29)	7.68E-04-1.04E-03 (5)	7.37E-04-1.18E-03 (18)
FcγRIIa/CD32a_R131 receptor binding affinity by BLI				
K_D (M)	1.37E-06-1.64E-06 (6)	7.67E-07-1.84E-06 (29)	1.19E-06-1.48E-06 (5)	7.32E-07-1.58E-06 (18)
k_a (1/Ms)	1.55E+05-1.79E+05 (6)	1.26E+05-2.31E+05 (29)	1.69E+05-1.97E+05 (5)	1.50E+05-2.32E+05 (18)
k_{dis} (1/s)	2.45E-01-2.62E-01 (6)	1.82E-01-2.74E-01 (29)	2.33E-01-2.73E-01 (5)	1.63E-01-2.71E-01 (18)
FcγRIIIa/CD16a_V158 receptor binding affinity by BLI				
K_D (M)	1.25E-07-1.63E-07 (6)	7.88E-08-1.89E-07 (28)	1.13E-07-2.06E-07 (5)	8.85E-08-2.05E-07 (18)
k_a (1/Ms)	3.62E+05-4.50E+05 (6)	2.90E+05-4.95E+05 (28)	3.37E+05-4.16E+05 (5)	2.67E+05-4.59E+05 (18)
k_{dis} (1/s)	5.61E-02-5.93E-02 (6)	3.42E-02-7.01E-02 (28)	4.70E-02-6.87E-02 (5)	3.69E-02-6.88E-02 (18)
ADCC activity	Not measurable (1)	Not measurable (1)	Not measurable (1)	Not measurable (1)
CDC activity	Not measurable (1)	Not measurable (1)	Not measurable (1)	Not measurable (1)

Table 6 Summary of the protein content and subvisible particle data of the IV and SC presentations of the RGB-19 proposed biosimilar and reference product RoActemra® batches

Attribute	RGB-19 IV Min-Max range (n)	RoActemra® IV Quality range (n)	RGB-19 SC Min-Max range (n)	RoActemra® SC Quality range (n)
Composition and strengths				
Protein concentration (mg/mL)	20.2-20.7 (6)	19.6-20.9 (47)	181.8-185.9 (5)	179.2-188.8 (33)
Subvisible particles				
Number of subvisible particles by LO (particles/vial)				
≥2 µm	2,713-11,149 (6)	4,841-17,560 (25)*	1,331-2,240 (5)	2,786-16,030 (17)*
≥5 µm	497-2,032 (6)	659-3,020 (25)*	185-399 (5)	607-2,762 (17)*
≥10 µm	53-252 (6)	11-285 (25)*	44-92 (5)	103-650 (17)*
≥25 µm	1-5 (6)	1-13 (25)*	12-30 (5)	5-399 (17)*
Number of subvisible particles by RMM (particles/mL)				
All particles	1.91E+05-7.10E+05 (6)	1.19E+05-2.50E+07 (30)*	1.95E+05-5.95E+05 (5)	9.04E+04-9.80E+06 (13)*
Protein related particles	9.03E+04-6.70E+05 (6)	2.00E+04-2.45E+07 (30)*	0-1.66E+04 (5)	0-1.75E+06 (13)*
Silicone like droplets	3.81E+04-1.46E+05 (6)	3.81E+04-1.50E+06 (30)*	1.79E+05-5.95E+05 (5)	9.04E+04-8.05E+06 (13)*

*Min-Max range is considered as quality range due to the large method variance